Amine infused hydrogel-based CO_2 gas storage technology for CO_2 hydrate-based cold thermal energy storage

Xiaolin Wang[a,*], Shufan Yang[a], Hai Zhang[b], Xingguang Xu[c,d], Colin Wood[e], Wojciech Lipiński[a]

a College of Engineering and Computer Science, The Australian National University, Canberra, ACT 2601, Australia
b Institute of Thermal Energy Engineering, School of Mechanical Engineering, Shanghai Jiao Tong University, Shanghai 200240, China
c Key Laboratory of Theory and Technology of Petroleum Exploration and Development in Hubei Province, China University of Geosciences, Wuhan 430074, China
d Key Laboratory of Tectonics and Petroleum Resources Ministry of Education, China University of Geosciences, Wuhan 430074, China
e CSIRO, Energy, Australian Resources Research Centre, Kensington, Western Australia 6151, Australia
*Corresponding authors: xiaolin.wang@anu.edu.au

Abstract: Carbon dioxide (CO_2) hydrate-based cold thermal energy storage (CTES) is a promising method for load shifting and demand management of cooling systems and for CO_2 utilisation. A challenge of CO_2 hydrate-based CTES is to find a compatible CO_2 gas storage, the CO_2 regeneration and absorption conditions of which can be coupled with the charging and discharging conditions of the CTES, respectively. Amine diethanolamine infused hydrogels (DEAIHs) can be an effective CO_2 absorber as the gas–DEA surface contact area is greatly enlarged by infusing the solution into a hydrogel. However, the influencing factors of the CO_2 absorption and regeneration performance of DEAIHs are unknown. This paper investigates the performance of DEAIHs and explores the possibility of applying them in cyclic CO_2 gas storage for CTES. The effects of pressure, temperature, DEAIH sample mass and amine diethanolamine (DEA) mass fraction on CO_2 absorption and absorption rate are investigated. It was found that a higher pressure prompted CO_2 absorption while a temperature of 12°C resulted in the highest CO_2 absorption rate. The average CO_2 absorption rates in the first 100 min were 0.250, 0.228, 0.155 and 0.033 mmol min^{-1} for 20-g DEAIH sample with 30-wt% DEA and 60-g DEAIH sample with 30, 47 and 89-wt% DEA, respectively. CO_2 regeneration from DEAIH under zero and non-zero gauge pressures are studied. Under non-zero gauge pressures, a pressure rise followed by a pressure drop caused by CO_2 re-absorption appeared in the CO_2 regeneration from DEAIH. It was found for the first time that the system passed through a meta-equilibrium state before it reached an equilibrium pressure. Cyclic absorption and regeneration at 110°C under zero gauge pressure showed that the CO_2 absorption decreased dramatically after the third cycle due to the volatility of amine. Operating a coupled CO_2 hydrate-based CTES and CO_2 gas storage system demonstrated the possibility of DEAIH material for CO_2 gas storage in CTES systems.

Keywords: amine infused hydrogels; gas hydrates; carbon dioxide storage; cold thermal energy storage

1 Introduction

Cold thermal energy storage (CTES) is used in cooling systems in which cooling capacity is produced at opportune times and later deployed for cooling services. The use of CTES in cooling systems can lower electricity costs by accessing off-peak electricity rates and lower the peak load on electricity grids. In addition, the chiller efficiency can be increased through night-time operation, and the chiller size and initial cost can be reduced by sharing the cooling load with CTES. Phase change materials (PCMs) enable CTES with large cooling storage capacity and relatively small footprint. However, they usually have high cost and stability issues [1].

CO_2 hydrates show superior properties compared to other PCMs, including: a phase equilibrium temperature that is relevant for air conditioning (AC) applications (0–20°C); high latent heat (501–507 kJ kg^{-1} for pure CO_2 hydrate [2] and 318.5–440.8 kJ kg^{-1} for CO_2 hydrate in the presence of promoters [3–5]); low material cost; safe operation and chemical stability. The phase equilibrium temperature can be adjusted by varying the composition and pressure, which is a unique property among PCMs. The cooling capacity storage (charge) and release (discharge) are realised by the exothermic gas hydrate formation process and the endothermic gas hydrate dissociation process, respectively. There is a number of works on different additives to improve thermodynamic properties of CO_2 hydrates, including tetra-n-butylammoniumbromide (TBAB) [6], tetrabutylphosphonium bromide (TBPB) [7] and tetrahydrofuran (THF) [8], etc. It was found that the addition of THF extended hydrate stability region by elevating equilibrium dissociation temperature and lowering pressure [8]. Adding TBAB and TBPB to the water at low concentration (TBAB at 5 wt% and TBPB at 0.58 mol%) decreased the pressure of CO_2 hydrate formation to nearly 5 bar at 9°C, instead of 35 bar at the same temperature in the absence of a promoter [6, 7]. In our previous work, by adding 32-wt% (2.56-mol%) TBAB, the phase equilibrium pressure was further reduced to 3.8 bar at 12.8°C [4]. The toxicity of TBAB is lower than that of TBPB and THF. The phase equilibrium conditions of CO_2–TBAB hydrate are shown in Table 1.

CO_2 hydrate crystals formed in a self-developed laboratory-scale CO_2 hydrate reactor are shown in Figure 1 [9]. In such a cold storage configuration, temperature was controlled by chilled water from a thermostatic bath, and pressure was adjusted by a regulator connected to a CO_2 gas cylinder [10]. This temperature-control method is widely implemented in hydrate formation studies. In the work of Gambelli [11], a chiller and glycol filled copper tubes were used for regulating the water-glycol bath to desired temperature to control the reactor temperature. By Yuan et al. [12] the reactor was immerged into a water bath containing a certain concentration of ethylene glycol to maintain constant temperature within the range of 253–353 K. The details of the manipulation was reported in our previous studies [13, 14].

Figure 1. CO_2 hydrate formed in a hydrate-based CTES [9].

In CTES systems, CO_2 gas storage is essential to temporarily store CO_2 released from gas hydrate dissociation, which is usually omitted from considerations in studies of CO_2 hydrate-based CTES. The released CO_2 is of a large amount, e.g. 0.5-m^3 CO_2 (STP) can be released from 10-kg CO_2–TBAB hydrate. A typical gas storage in a CTES–AC system is shown in Figure 2, which can significantly increase the system size and initial cost. The space-footprint and capital cost of gas storage can be greatly reduced if compatible CO_2 sorbents are employed in the CO_2 storage. The desired characteristics of sorbents should enable cost-effective and reversible CO_2 absorption–regeneration cycling at suitable pressure–temperature conditions with a large volumetric reduction of CO_2 gas.

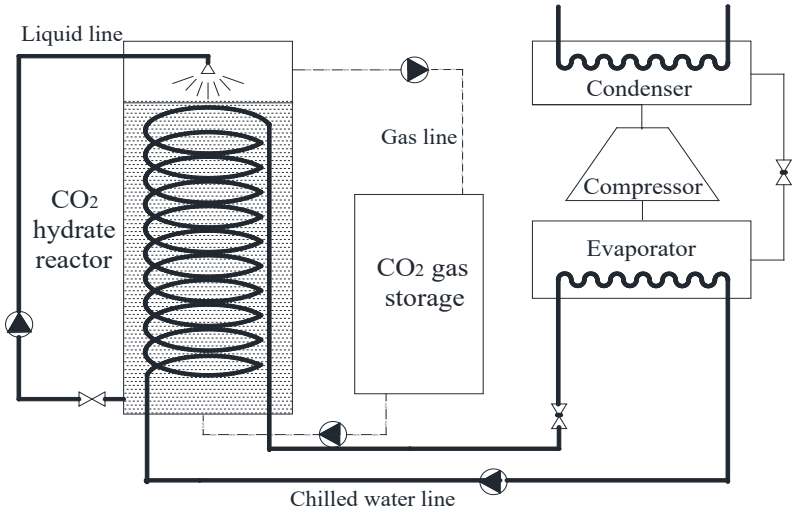

Figure 2. Schematic of a typical CO_2 hydrate-based CTES system with CO_2 gas storage.

Table 1 CO_2–TBAB hydrate experimental conditions [4]

TBAB wt%	T_{equ} (°C)	P_{equ} (bar)	TBAB wt%	T_{equ} (°C)	P_{equ} (bar)	TBAB wt%	T_{equ} (°C)	P_{equ} (bar)
10			20	13.0	9.02	32	14.3	9.14
	11.0	6.83		12.7	7.33		14.1	6.70
	10.6	5.98		12.4	6.38		13.6	5.50
	9.70	4.73		12.1	5.53		13.2	4.70
	8.65	3.83		11.6	4.48		12.8	3.83
	6.70	2.50		10.2	2.80		11.9	2.20

Suitable CO_2 sorbents to reduce gas storage capital and operational cost are to be explored before any CO_2 gas hydrate-based CTES can be prototyped for commercial use. In general, each system has its unique requirements for CO_2 absorption and regeneration conditions. A CO_2–TBAB hydrate-based CTES requires the absorption to be applicable at around 7°C and 10 bar and the corresponding regeneration at >12°C and 5 bar [13, 14]. However, not a CO_2 sorbent meeting these requirements are commercially available. Commonly-used methods include physical adsorbents [15–18] and chemical absorbents [19–23]. In physical adsorptions, CO_2 molecules are retained on the surface of the solid matrix of a porous medium [16, 24], such as porous carbons [25–32], metal organic frameworks [33], hypercrosslinked polymers [18, 34] and covalent organic polymers [35] with high adsorption capacity and selectivity, easy regeneration, and high thermo-chemical stability. However, these materials are expensive and the adsorption is negatively impacted by the presence of water. Chemical absorption usually adopts liquid amines that react with CO_2, which is cost-effective. However, it is usually achieved in a high space-footprint plant that can cycle the liquid amine. CO_2 capture by aqueous amine scrubbing has been widely accepted by the industry owing to its maturity, economy, and extensive applicability in related industrial applications such as acid gases removal from natural gas [36, 37]. The reaction mechanism of CO_2 absorption by primary and secondary amines is referred to as carbamate hydrolysis. The regeneration of stored CO_2 from liquid amine is an energy intensive process due to high regeneration temperatures. The process adds significant operating cost to the process and leaves a considerable carbon footprint itself [36]. The regeneration at high temperatures also causes amine to evaporate. Another drawback of amine-based CO_2 storage is the heavy diffusion limitation between CO_2 and amine, compared to most solid adsorbents such as zeolites and MOFs [38]. The reaction between amine solution and CO_2 to form carbamate is

$$\text{CO}_2 \text{ absorption: } 2\text{R}_1\text{R}_2\text{NH} + \text{CO}_2 \rightarrow \text{R}_1\text{R}_2\text{NH}_2^+ + \text{R}_1\text{R}_2\text{NCOO}^- + \text{heat} \quad (1a)$$

$$\text{CO}_2 \text{ regeneration: } \text{R}_1\text{R}_2\text{NH}_2^+ + \text{R}_1\text{R}_2\text{NCOO}^- + \text{heat} \rightarrow 2\text{R}_1\text{R}_2\text{NH} + \text{CO}_2 \quad (1b)$$

Amine absorbents can be combined effectively with solid porous media to enlarge CO_2–amine contact surface to alleviate the diffusion limitation and improve CO_2 absorption, i.e. amine-functionalised sorbents [39–42]. They comprise a support, typically porous, with weakly bonded pre-made polymeric amines or small amine molecules or with covalently bonded small amine molecules or in situ formed polymeric amines [36]. These supports usually have large surface areas and pore volumes so that the CO_2 absorption kinetics and capacity can be significantly improved compared to that of liquid amines. However, fabrication of supports can be complex, and they may exhibit poor selectivity towards CO_2 [38]. A new CO_2 sorbent was developed Xu et al. [43] by adding commercially available hydrogels into organic amine solutions to generate amine infused hydrogels (AIHs). AIHs could rapidly absorb CO_2 with a high absorption capacity even in the absence of mechanical agitation with a stable cyclic performance.

Although AIHs are promising as inexpensive and readily available CO_2 sorbents, the absorption performance under various pressures, temperatures and different amine concentrations is unknown. In addition, there is no proof-of-concept study on the viability of an AIH-enabled CO_2 gas storage to assist in the cyclic operation of a CO_2 hydrate-based CTES system. In the present work, we extend the study by Xu et al. [43] to infuse a secondary amine diethanolamine (DEA) of a commercially available hydrogel for CO_2 storage. Fourier-Transform Infrared (FTIR) spectroscopy is performed to obtain transmission spectra of DEA infused hydrogels (DEAIH) before and after absorption and regeneration runs. We investigate the CO_2 absorption and absorption rate of DEAIH at various DEAIH sample mass, DEA concentrations, temperatures and pressures. The factors influencing CO_2 regeneration and DEAIH cyclic performance under zero and non-zero gauge pressures are investigated. A coupled CO_2 hydrate-based CTES and DEAIH-based CO_2 storage system is developed in a laboratory. CO_2 gas regeneration–CO_2 hydrate formation and CO_2 hydrate dissociation–CO_2 gas adsorption are executed in a cyclic operation to experimentally evaluate the system performance.

2 Experimental system and procedure

2.1 Materials

The materials used in the experiments are reported in Table 2. DEA was selected as the standard amine due to its high reactivity and low volatility, with the latter a major problem for amines scrubbing in stripper columns [43]. The choice to use poly(acrylamide-co-acrylic acid) potassium as the base hydrogel material was for its

good gelation strength, swelling behaviour, small weigh loss due to thermal degradation, low sensitivity to temperature, pH and salinity changes [44]. It has been tested to show thermal stability up to 300°C [43].

Table 2. Materials for the experiment

Material	Property
DEA (Sigma-Aldrich)	Purity 99%
Poly(acrylamide-co-acrylic acid) potassium salt (Sigma-Aldrich)	Particle size 200 μm
CO_2 gas (BOC Gases)	Purity 99%

2.2 Experimental setups and procedures

2.2.1 CO_2 absorption

To study the influencing factors of DEAIH absorption performance towards CO_2, experiments were conducted in a CO_2 storage cylinder, with an internal volume of 196 mL, which consisted of a brass cylinder with two 25-mm thick polycarbonate panels on top and at the bottom, as shown in Figure 3. It had eight stainless steel bolts to tightly hold the polycarbonate panels with O-rings, which enabled it to sustain a pressure to 6.89 MPa according to calculation and simulation results. The CO_2 storage cylinder was put in a thermostatic air chamber for controlled ambient temperature, as shown in Figure 3. The temperature and pressure in the CO_2 storage cylinder were measured by a calibrated platinum resistance and a calibrated pressure sensor, respectively, and were collected by a data acquisition system with a time interval of 5 seconds. The systematic error of the temperature measurement was ±0.1°C and that of pressure measurement was ±0.005 bar.

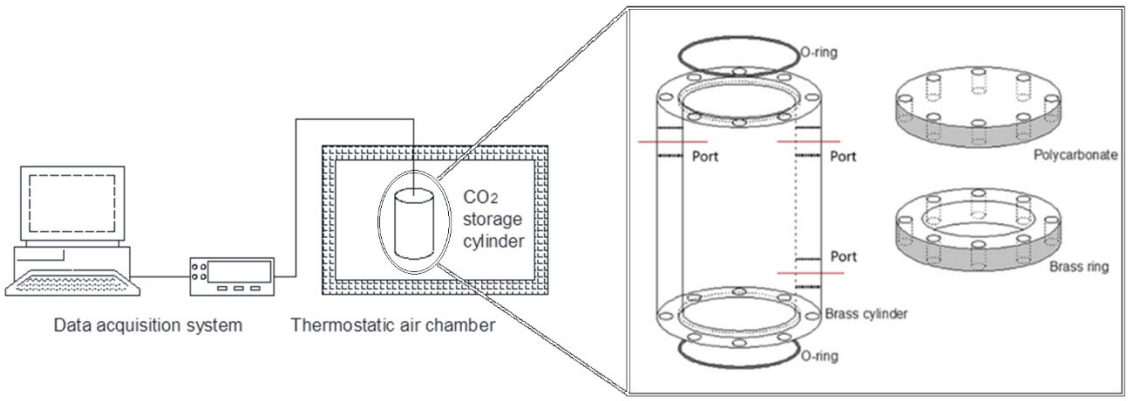

Figure 3. Experimental setup.

IR transmittance spectra were obtained using a Bruker ALPHA FTIR spectrometer. A background scan of air was first performed. All tests were carried out under ambient conditions and the diamond surface was thoroughly cleaned with ethanol before each measurement. The spectra were recorded by a data acquisition system.

The influencing factors studied included DEAIH sample mass, DEA concentration in the solution, CO_2 feed pressure, and ambient temperature. All variables in this study are listed in Table 3. In the preparation of DEAIHs with high-concentration DEA, 30-wt% DEA solutions were infused into hydrogels and then the DEAIH samples were dried in a desiccator to make sure DEA was uniformly distributed in the hydrogels. Weight measurements were repeated until the desired DEA concentration was reached. The appearance of DEAIHs at different DEA concentrations are shown in Figure 4. The DEAIH sample with a high DEA concentration was obviously firmer and darker.

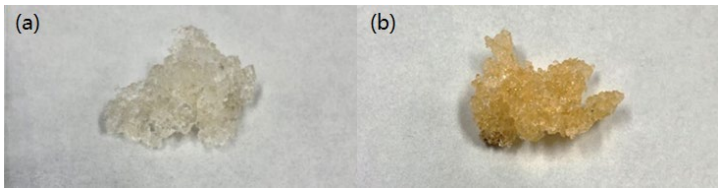

Figure 4. DEAIHs with DEA concentration: (a) 30 wt% and (b) 86 wt%.

Table 3. Conditions applied in the absorption and regeneration experiments

Operation	Fixed parameters	Variables
Sorption	DEA 30 wt%, 3 bar, 23°C	20g
		60g
	60 g, 3 bar, 23°C	30 wt%
		47 wt%
		89 wt%
	60 g, DEA 30 wt%, 23°C	1 bar
		2 bar
		3 bar
	60 g, DEA 30 wt%, 3 bar	5°C
		12°C
		23°C
Regeneration	15 g, DEA 30 wt%, 0 bar	90°C
		100°C
		110°C
		120°C
	90 g, DEA 30 wt%, 90°C	1.5 bar
		3.0 bar

2.2.2 CO_2 regeneration

The regeneration of CO_2 from DEAIH was conducted under two different cases: under zero gauge pressure and non-zero gauge pressures. For tests under zero gauge pressure, the regeneration experiments were conducted in a gravity convection oven (EQ-DHG-9245A) at a fixed temperature with each 15-g CO_2-loaded DEAIH sample (30 wt%) contained in a glass vial for four hours. The selected regeneration temperatures in this experiment were 90, 100, 110 and 120°C, as shown in Table 3. For tests under non-zero gauge pressures, the samples of 90 g and 30 wt% were placed in the CO_2 storage cylinder under different initial pressures: 1.5 and 3.0 bar, as shown in Table 3. This was achieved by charging the cylinder containing DEAIH with CO_2 under constant pressure to DEAIH's full capacity. The cylinder was placed in the gravity convection oven for heating and the temperature and pressure of gas in the cylinder were measured continuously. Cyclic absorption and regeneration processes were operated with 1-hour CO_2 absorption, 3-hour regeneration at 110°C under zero gauge pressure, and 1-hour hydrogel recovery with compensating water enhanced by ultrasound. The sample from each regeneration was cooled to ambient temperature before the following absorption. Multiple cycles were performed to evaluate the recyclability of the prepared DEAIHs as reported in [38, 43].

2.2.3 Coupled system of CO_2 hydrate-based CTES and CO_2 gas storage

As can be seen in Figure 5, the coupled system was composed of a CO_2 hydrate reactor and a CO_2 gas storage cylinder, connected by a soft pipe. The CO_2 hydrate reactor had a total inner volume of 62.5 mL, the gas storage had an inner volume of 196 mL, and the pipe accounted for 14 mL. There were two valves between the two pressure vessels on each side of the pipe. The gas storage was initially fed with 90-g DEAIH. The CO_2 hydrate reactor was filled with 35-g TBAB water solution (32 wt%) from the liquid inlet. This TBAB concentration was selected from previous results for a suitable phase change temperature and large formation enthalpy according to the formula of $2.51CO_2$+TBAB+$38H_2O$, which corresponds to the stoichiometric ratio of TBAB in water of 32 wt% [4, 45]. The rated hydrate formation is 38.8 g with 3.80 g hydrated CO_2.

The cyclic operation of the coupled system of CO_2 hydrate-based CTES and CO_2 gas storage consists of following steps (Figure 6): (1) charge DEAIH in CO_2 storage cylinder with CO_2 to its full capacity; (2) manually place the CO_2 storage cylinder in a high-temperature thermostatic bath to regenerate CO_2 from DEAIH; (3) when the pressure in the CO_2 storage cylinder reaches a peak, the valves to the CO_2 hydrate reactor are opened to let CO_2 in; (4) when the pressure in both pressure vessels are equal, the valves are closed to separate the two vessels; (5) manually move the CO_2 storage cylinder from the high-temperature thermostatic bath to the ambient air for cooling down; (6) the CO_2 hydrate reactor is cooled in a thermostatic bath for CO_2–TBAB hydrate formation;

(7) after hydrate formation ceases, the CO_2 hydrate reactor is heated in the thermostatic bath to dissociate CO_2–TBAB hydrate; and (8) when the pressure in CO_2 hydrate reactor is stable, the valves are opened again to allow released CO_2 to be absorbed by DEAIH. When an equilibrium is reached, a cycle is hereby complete as the state of CO_2 in the storage cylinder, after a following regeneration, can provide sufficient pressurised CO_2 for the next CO_2 hydrate formation. This will be illustrated in section 4.6.

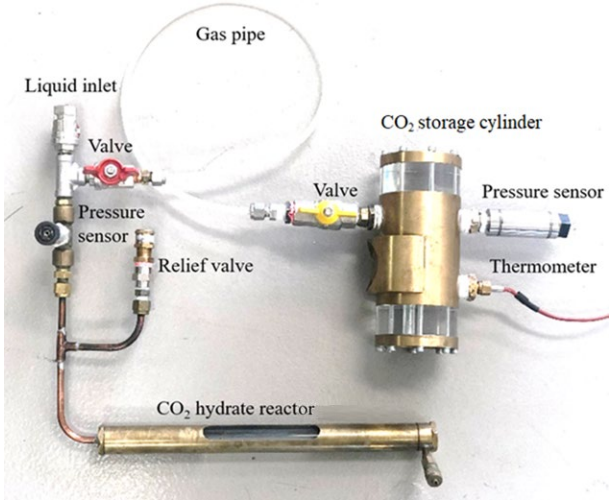

Figure 5. Coupled system of CO_2 hydrate reactor and DEAIH-based CO_2 gas storage.

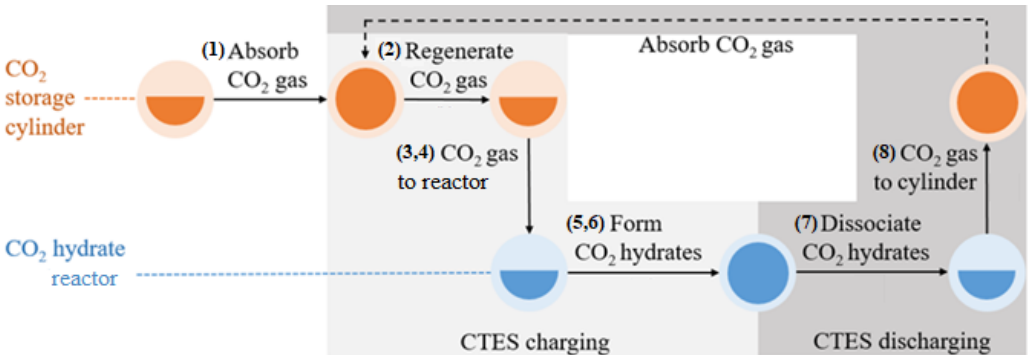

Figure 6. Operation of the coupled system of CO_2 hydrate-based CTES and CO_2 gas storage.

3 Analysis

The amount of absorbed CO_2 in the storage cylinder can be calculated as

$$n_{CO_2,abs} = n_{CO_2(g),1} - n_{CO_2(g),2} \tag{2}$$

where $n_{CO_2(g),1}$ and $n_{CO_2(g),2}$ are the amount of gaseous CO_2 in state 1 and 2, respectively. The normalised CO_2 absorption is calculated as

$$\overline{n}_{CO_2,abs} = \frac{n_{CO_2,abs}}{m_{DEA}} \tag{3}$$

where m_{DEA} is the mass of DEA in the hydrogel. The mass of CO_2 regeneration under zero gauge pressure can be determined from

$$m_{CO_2,reg} = m_{loss\_total} - m_{loss\_H_2O} \tag{4}$$

where m_{loss_total} and $m_{loss\_H_2O}$ are the mass loss of the sample with absorbed CO_2 and the reference sample of DEAIH without having absorbed CO_2 during the whole regeneration period, respectively. CO_2 regeneration under non-zero gauge pressures is calculated as

$$n_{CO_2,reg} = n_{CO_2(g),2} - n_{CO_2(g),1} = \left(n_{total(g)} - n_{H_2O(g)}\right)_2 - \left(n_{total(g)} - n_{H_2O(g)}\right)_1 \quad (5)$$

where the amount of all gaseous components $n_{total(g)}$ in state 1 and 2 are found using the ideal gas equation. The vapour pressure in the closed system is calculated using the Antoine equation.

$$\log_{10} P = A - \frac{B}{T + C} \quad (6)$$

where the parameters A, B and C are equal to 8.07131, 1730.63 and 233.426, respectively. For water vapour at 100°C, T is in °C and P is in mmHg. The amount of water vapour in the gas mixture $n_{H_2O(g)}$ in both states are found from the partial pressure using the Dalton model. The normalised CO_2 regeneration is

$$\overline{n}_{CO_2,reg} = \frac{n_{CO_2,reg}}{m_{DEA}} \quad (7)$$

CO_2 solubility in water is calculated using the model of Henry's law [46, 47]. It is assumed that the activity coefficients for both solvent and solute are unity and the Poynting correction is negligible [48]. The solubility of CO_2 in water is not altered by the presence of hydrates [49]. The detailed equations are presented in our previous works and has been verified for CO_2 gas hydrates with additives [4, 5]. The gas in hydrate was found according to CO_2 mass balance in the hydrate reaction tube. The CO_2 mass balance in the whole system can be expressed as

$$n_{CO_2,total} = n_{CO_2(g)} + n_{CO_2(dissolved)} + n_{CO_2(hyd)} + n_{CO_2(DEAIH)} \quad (8)$$

where $n_{CO_2(dissolved)}$, $n_{CO_2(hyd)}$ and $n_{CO_2(DEAIH)}$ are the amount of CO_2 dissolved in water, hydrated, and stored in DEAIH, respectively. The detailed chart of the calculation process is shown in Figure 7.

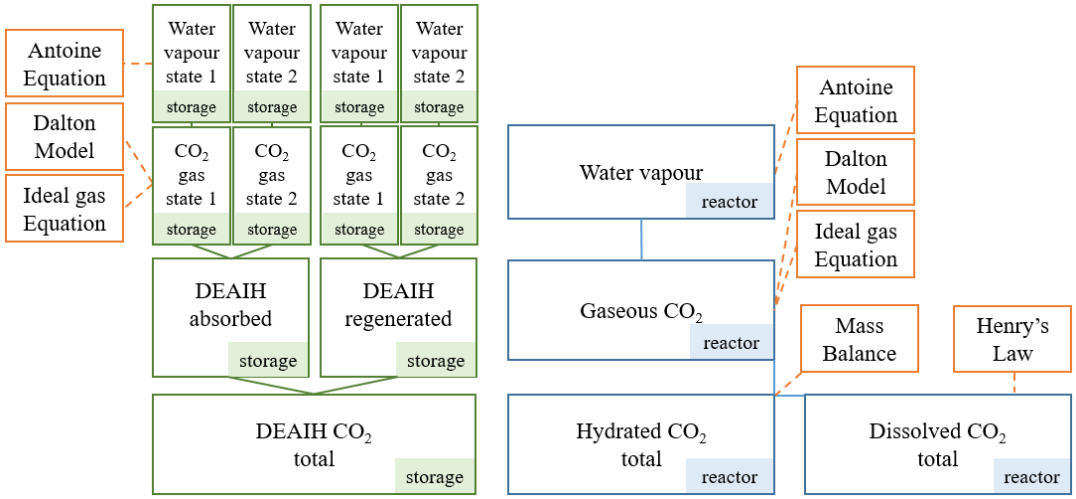

Figure 7. Chart of amount of CO_2 calculation in different parts of the experimental system.

4 Results and discussions

4.1 FTIR analysis

Spectral transmittance of DEAIH with amine concentration of 30 wt% before and after CO_2 absorption and regeneration was measured to elucidate the reaction between CO_2 and DEAIHs, as shown in Figure 8. Peaks or plateaus were observed at wavenumbers of 3330, 3200, 2840–2950, 1550, 1400 and 1040–1070 cm^{-1} corresponding to O–H stretching, N–H stretching, C–H stretching, O–H bending, C–H_2 bending and C–N stretching. The bands are highlighted in Figure 8. The main indicator of the carbamate formation was the presence of COO^- [38]. New bands appeared at around 1500 and 1260 cm^{-1} after CO_2 absorption, which corresponds to the asymmetric and symmetric COO^- stretching, respectively [50, 51]. These characteristic bands were not present before CO_2 was introduced, indicating the absence of the DEA carbamate.

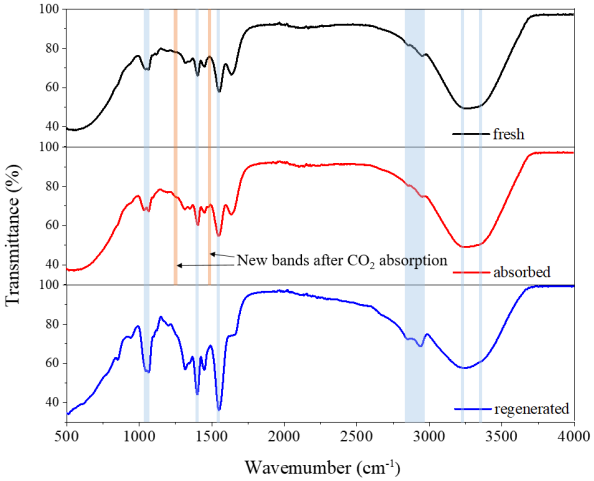

Figure 8. Transmittance spectra of fresh DEAIH (black), DEAIH after CO_2 absorption (red), and DEAIH after regeneration (blue).

4.2 CO_2 absorption

In a CO_2 hydrate-based cold storage operation, CO_2 is gradually released during discharge and thus the excess reactant is always the CO_2 absorbent. Therefore, the absorption experiment in the CO_2 storage cylinder in the study was with excess DEA. The effects of DEAIH sample mass are shown in Figure 9a indicating that with a same amount of CO_2 gas in the closed cylinder, a larger amount of DEAIH resulted in higher CO_2 absorption and absorption rate. The average CO_2 absorption rates in the first 100 min were 0.110 and 0.041 mmol min^{-1} for 60 g and 20 g DEAIH, respectively. The effects of DEA concentration are illustrated in Figure 9b, showing a slight difference of CO_2 absorption between 30 wt% and 47 wt% but a dramatically lower CO_2 absorption at 89 wt%. The average absorption rates in the first 100 min were 0.111, 0.109 and 0.043 for 30, 47 and 89 wt% DEA, respectively. The reason might be that the lower amount of water and the firm character of 89 wt% DEA sample limited the diffusion of CO_2 into DEAIH. The CO_2 absorption of 47-wt% DEA sample is higher than that of the 30-wt% DEA sample, since a higher DEA concentration in water provided more R_1R_2NH molecules for the reaction, and the physical character of the 47-wt% DEA sample did not cause an obvious restraint on CO_2 diffusion. As seen in Figure 9c, the highest CO_2 absorption rate was achieved at 12°C experimental temperature, which was very close to the rate at the room temperature of 23°C in the first 45 min. The lowest CO_2 absorption rate was found in the run at 7°C, in which the CO_2 absorption kept increasing until the end of experiment. The average absorption rates in the first 100 min were 0.149, 0.144 and 0.065 mmol min^{-1} for 23, 12 and 7°C, respectively. Comparing 12 and 23°C, a lower ambient temperature is more favourable as the CO_2 absorption reaction is an exothermic reaction. On the other hand, DEA is a viscous liquid and its viscosity increases dramatically with reduced temperature [52]. It is believed that the viscosity of DEA at around 7°C reached a critical value to impose a major restraint on CO_2 mass transfer, which may be the reason for the great reduction in CO_2 absorption at 7°C. However, further studies are required to verify this speculation. Figure 9d shows that increasing the CO_2 pressure from 1 bar to 2 bar significantly raised the CO_2 absorption by 86.6%. A further increase in CO_2 pressure from 2 bar to 3 bar only resulted in 6.6% increase of CO_2 absorption. Pressure is a driving force of transport phenomena. In the CO_2 absorption, when CO_2 mass transfer into DEAIH is weak under low pressures, increasing the pressure will dramatically improve the mass transfer; while when mass transfer is dominant, the absorption will no longer be enhanced obviously by increasing the pressure. The average absorption rates in the first 100 min were 0.035, 0.072 and 0.069 mmol min^{-1} for 1, 2 and 3 bar, respectively. In general, initially the CO_2 absorption rate was high, but subsequently dropped to 0.005–0.015 mmol min^{-1} after 100 min and remained approximately constant to the end of the absorption.

The normalised CO_2 absorption was used to study the absorption performance. The results are shown in Figure 10. A smaller size of the DEAIH sample dramatically increased the CO_2 absorption and absorption rate as a much larger contacting surface was provided. At DEA concentrations above 30 wt%, a lower DEA concentration was favourable to maintain a high CO_2 absorption and rate. On one hand, water provides a better

CO_2 diffusion into the hydrogels. On the other hand, CO_2 reacts in an acid-base buffer mechanism with alkanolamines in aqueous solutions, in which water plays an important role by providing hydrogen ion and the hydrolysis reaction of CO_2 [53]. DEA has a hydrogen atom directly bonded to nitrogen, showing intermediate properties compared to primary amines that react directly with CO_2 to form carbamate [54]. This necessitates the presence of a proper amount of water. Overall, the average CO_2 absorption rates in the first 100 min were 0.250, 0.228, 0.155 and 0.033 mmol min^{-1} for 20-g DEAIH sample with 30-wt% DEA and 60-g DEAIH sample with 30, 47 and 89-wt% DEA, respectively.

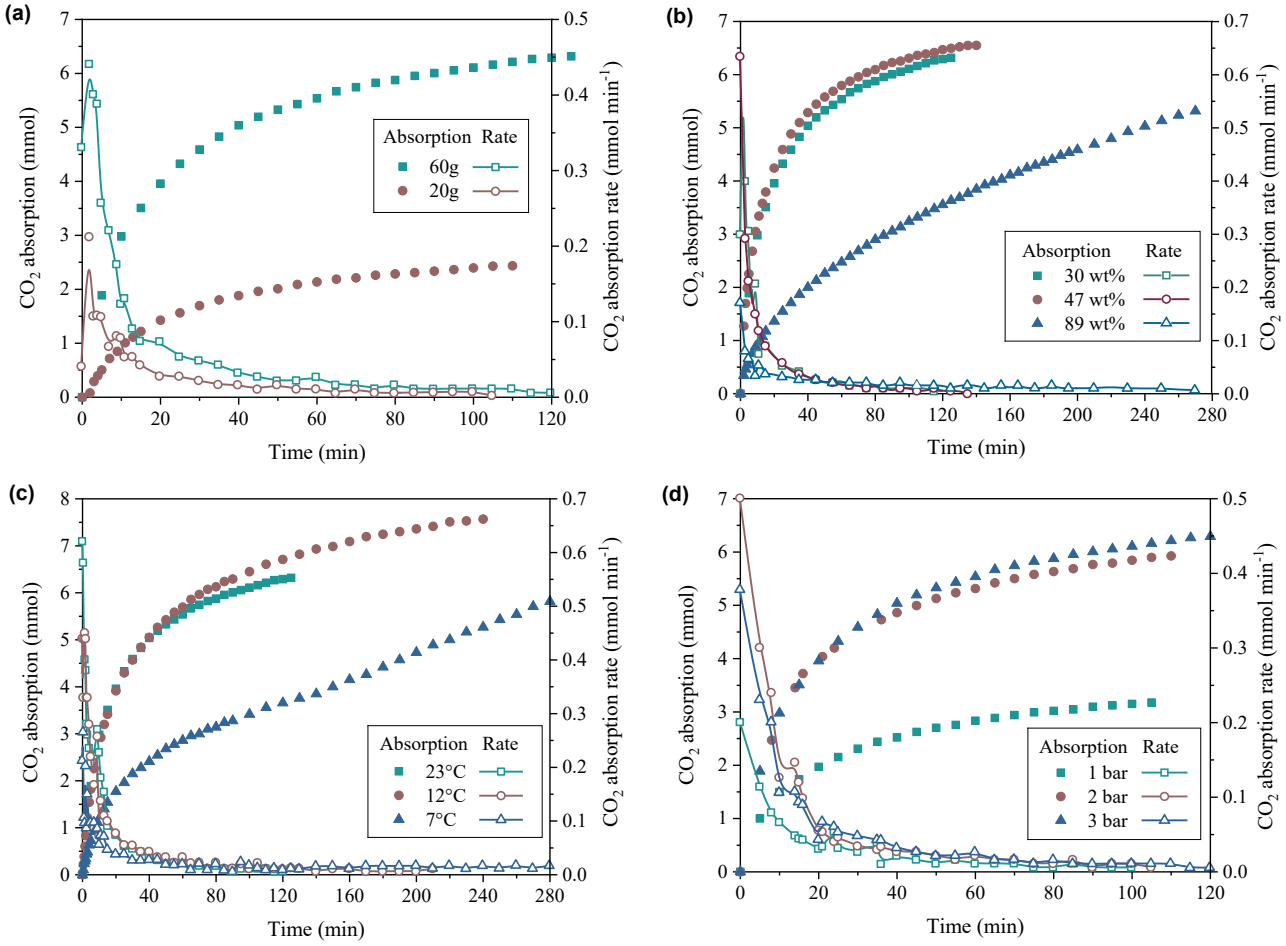

Figure 9. Effects of (a) DEAIH sample mass, (b) DEA concentration, (c) ambient temperature and (d) pressure of the CO_2 storage cylinder on CO_2 absorption and absorption rate.

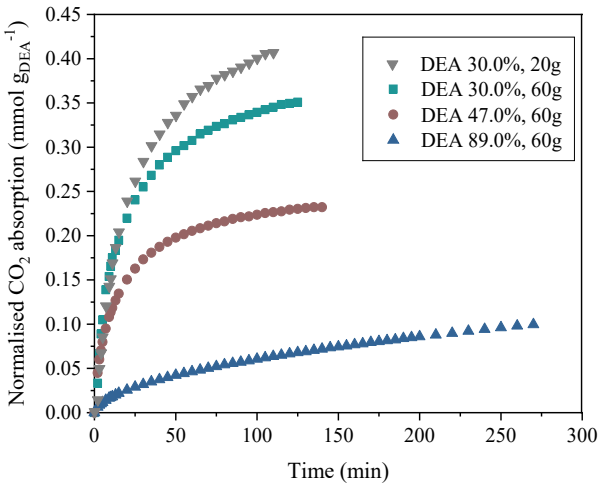

Figure 10. Normalised CO_2 absorption for selected DEAIH sample mass and DEA concentrations.

4.3 CO_2 regeneration process under zero gauge pressure

The reaction of CO_2 regeneration from amine is an endothermic reaction. The regeneration heat comprises the sensible heat which is necessary to bring amine to the regeneration temperature, and the latent heat of which the absolute value equals to the heat of regeneration and which is needed to overcome the chemical bonding strength between absorbed CO_2 and amine [55]. In this study, the regeneration process was conducted using 15-g samples of DEAIH (30 wt%) with CO_2 absorbed at 3 bar and ambient temperature. Continuous gas injection was performed to ensure CO_2 absorption in DEAIH at its full capacity. It was conducted by heating the samples in the gravity convection oven at constant temperatures for 4 hours, with the DEAIH sample mass measured every 30 min. The loss of mass due to CO_2 regeneration and water evaporation are presented in Figure 11. The DEAIH sample mass dropped approximately in a linear manner. The majority of mass loss resulted from water evaporation.

The normalised CO_2 regeneration at different regeneration temperatures are compared in Figure 12. The relative increase of the mass of regenerated CO_2 along with temperate rise per 10°C is shown. The mass of regenerated CO_2 at 100°C was 130.6% higher than that at 90°C. The mass at 110°C was 51.34% higher than that at 100°C. However, the mass at 120°C was only 11.26% higher than that at 110°C. Consequently, the optimum regeneration temperature among those reported in Figure 12 is 110°C, which is identified by taking into account both the effectiveness and the heating energy cost.

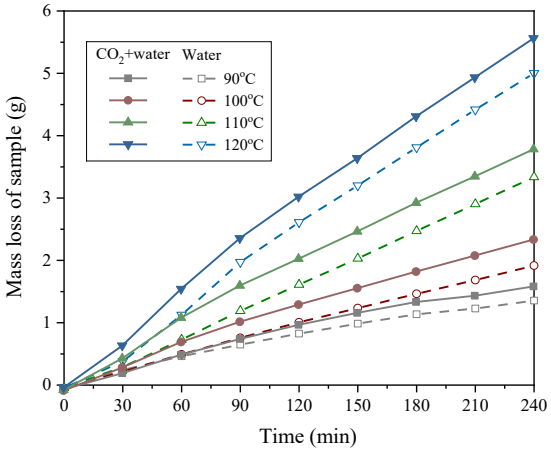

Figure 11. Mass loss of DEAIH samples due to water and CO_2 loss under zero gauge pressure.

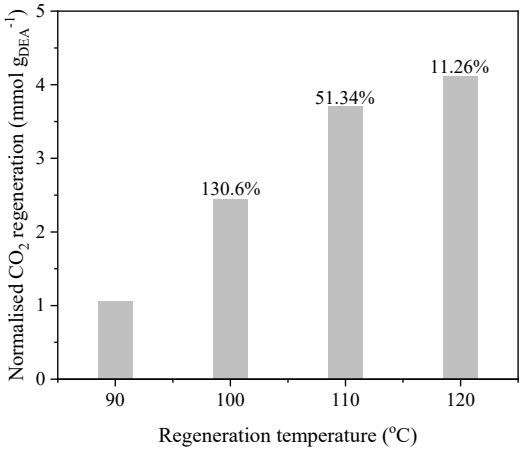

Figure 12. Normalised CO_2 regeneration at selected temperatures under zero gauge pressure.

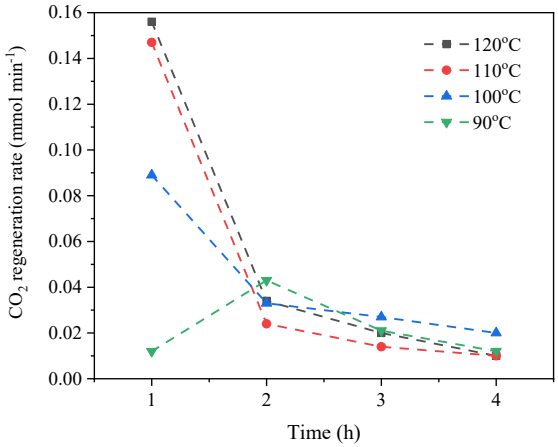

Figure 13. CO_2 regeneration rate at selected regeneration temperatures under zero gauge pressure.

The CO_2 regeneration rate at various regeneration temperatures are shown in Figure 13. At 110 and 120°C, the regeneration process had a very high rate (around 0.150 mmol min^{-1}) in the first hour. However, the regeneration rate dropped dramatically after that and became nearly zero at the end. Therefore, at temperatures above 110°C, the regeneration process is suggested to cease in around two hours for energy saving. At 100°C, the regeneration rate was only half of those at higher temperatures in the beginning and was maintained above 0.020 mmol min⁻

[1] till the end. At 90°C regeneration temperature, the rate was very low at the start. It increased in the second hour slightly and decreased again. For all the runs, the regeneration rate was very low after four hours indicating the regeneration reached to its full capacity.

4.4 Regeneration process under non-zero gauge pressures

A pressurised CO_2 regeneration process from DEAIH was carried out under 1.5 and 3 bar initially in the CO_2 storage cylinder. 90-g fresh DEAIH was charged with CO_2 to its full capacity under the corresponding pressure before being put in the cylinder. The cylinder was then placed in a thermostatic bath to perform regeneration at a constant temperature of 90°C. The cylinder was closed during the entire regeneration process. The pressure variation during the regeneration process of the run initially under 1.5 bar is shown in Figure 14. As can be seen, the pressure in the cylinder first rose until it reached a peak of 7.4 bar at 61 min, which is due to the regenerated CO_2 gas and possibly evaporated water at 90°C. It was followed by a sudden and steep pressure drop in 5 min, which is believed to be caused by the re-absorption of CO_2 in DEAIH at the high-pressure condition of 7.4 bar. It is noted that both CO_2 absorption and regeneration are affected by temperature and pressure, so there is an equilibrium state between absorption and regeneration which is determined by the pressure and temperature condition. The pressure decreased to 2.3 bar at 66 min and then it started to rise again. This reveals that, at the performed temperature condition of 90°C, the lowest pressure to initiate re-absorption is around 7.4 bar and the highest pressure to allow regeneration to start is about 2.3 bar. From 66 min, the system passed through a meta-equilibrium period until it reached an equilibrium pressure at 3.4 bar, indicated by the plateau in the pressure where the pressure changing rate approached 0. A similar trend was observed in the regeneration under initially 3 bar. However, it is unknown whether the trade-off between re-absorption and regeneration is determined by the global pressure or CO_2 partial pressure. This trade-off was not observed in the regeneration under zero gauge pressure.

The CO_2 regeneration under 1.5 and 3 bar are shown in Figure 15, compared with that under zero gauge pressure. The amount of CO_2 regeneration is calculated as the average of two measurements. The amount of regenerated CO_2 decreases evenly as the pressure increases. The CO_2 regeneration reduced by 37% when decreasing the pressure from 3 bar to 1.5 bar, and then reduces by 25% when decreasing the pressure from 1.5 bar to 0. This observation reveals that within the studied pressure range, CO_2 regeneration is subdued by the gauge pressure.

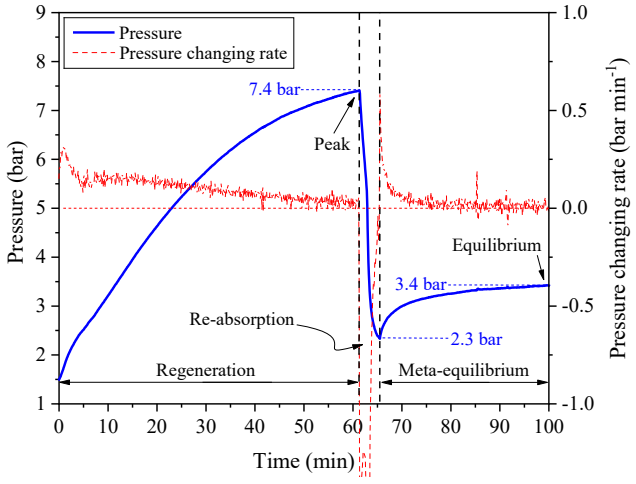

Figure 14. Pressure and pressure changing rate during CO_2 regeneration initially under 1.5 bar.

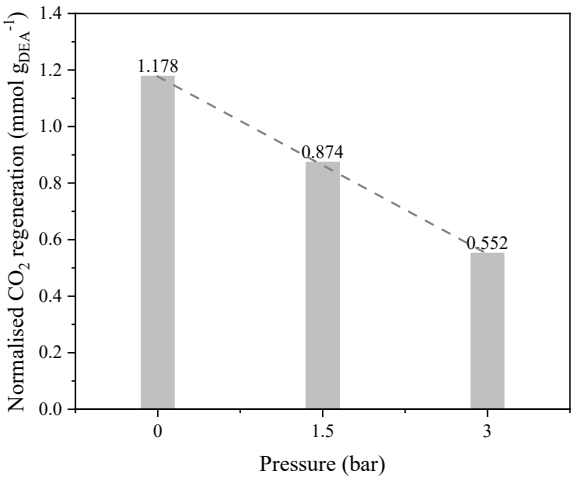

Figure 15. Normalised CO_2 regeneration under different gauge pressures.

Noted from result of DEAIH regeneration performance under both zero or non-zero gauge pressures, it is found that the regeneration should be triggered at above 90°C. This elevated temperature may result in concerns about energy efficiency of this application given the big gap between AC cooling temperature and DEA regeneration temperature. In fact, in terms of other CO_2 sorbent in both solid and liquid forms, temperature has to be elevated for regeneration. For example, temperature swing adsorption was employed for zeolites as the regeneration method through heating up to a temperature of approximately 100°C, and there was no full reversibility for zeolites [56]. More attempts of CO_2 regeneration from zeolite were performed at 150, 200, and 250°C [57]. Some metal–organic frameworks (MOFs), such as MOF-177, failed to exhibit a positive working capacity even

at regeneration temperatures as high as 200°C [58]. On the other hand, fabrication of these supports is complex and costly which has hindered large-scale operation. In addition, the performance of some of these sorbents can be degraded in the presence of water vapour that is abundant in the flue gas and hydrate-based CTES systems [38]. These can be overcome by using AIHs. For practical systems, the temperatures above 90°C are comparable or below the temperatures found in demonstration and commercial systems, such as direct air capture [59] and solar thermochemical CO_2 capture [60]. On the other hand, although the temperature swing method is energy consuming, this application with low and relatively high temperature parts can still be efficient if implemented with low-cost heat sources for CO_2 regeneration. An example is solar thermal adsorption or absorption cooling system with chilled water for CO_2 hydrate-based CTES and solar hot water for CO_2 regeneration.

4.5 Cyclic performance of CO_2 absorption and regeneration

The mass of regenerated CO_2 in five cycles is shown in Figure 16. The mass of regenerated CO_2 in the first cycle is taken as 100%, and that of the following cycles is calculated through Equation (4). The CO_2 absorption capacity of DEAIH decreased after cycles, which was primarily attributed to the volatility of DEA (boiling point 280 °C), as was reported in literature [38]. However, the cyclic performance in the present study was worse than the reported DEAIH with 20 wt% DEA that CO_2 absorption was as much as 78% of the original value after 10 cycles [38]. This is due to the higher water loss in open systems, higher regeneration temperature and longer regenerating time in the present study. The DEAIH sample mass may also influence the cyclic performance.

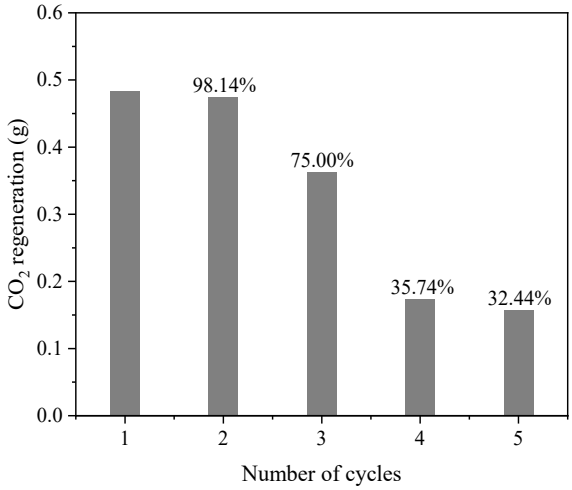

Figure 16. CO_2 regeneration during cycles under zero gauge pressure.

4.6 Coupled CO_2 hydrate thermal storage and CO_2 gas storage

The temperature and pressure variations in the storage and reactor during a complete operation are shown in Figure 17. Initially, the gas storage cylinder loaded with CO_2 to its full capacity was heated in a thermostatic bath for regeneration and the temperature in the cylinder was maintained at around 90°C. 90°C was selected in this study as a water bath was used for the coupled system experiment for a moderate the capital and operational cost. In practical systems, there is another option to use steam for the regeneration, which can be more applicable to reach the ideal regeneration temperature as well as sustain water saturation in the DEAIH. The pressure in the cylinder increased from 4.10 to 11.2 bar. From previous results of regeneration under non-zero gauge pressures, the pressure rise was followed by a sudden pressure drop due to CO_2 re-absorption. Therefore, in the coupled system, when a peak in pressure was observed, the valves between the reactor and gas storage cylinder were immediately opened to allow regenerated CO_2 to transport to the reactor for CO_2 hydrate formation. The valves were closed when the pressure in the reactor and cylinder were equal to make both vessels closed systems. The pressure in the reactor before hydrate formation was 6.64 bar. The reactor was then cooled in the thermostatic bath at 12.5°C. It was observed that the pressure in the reactor first dropped to 5.66 bar at 145 min due to CO_2 dissolution in water. It was followed by an abrupt pressure drop for CO_2–TBAB hydrate formation. Meanwhile, the temperature of the CO_2 gas storage cylinder reduced gradually to the ambient temperature. At 339 min, when pressure in the reactor dropped to 4.40 bar the hydrate dissociation was initiated by setting the thermostatic bath temperature to 30°C. As the CO_2–TBAB hydrate was dissociated, CO_2 gas was released, resulting in a pressure rise in the reactor. When the pressure became constant in the reactor, the valves were opened again to allow dissociated CO_2 to be absorbed by DEAIH in the gas storage cylinder. It was found that

at the point of opening valves, the pressure in the whole system immediately reduced to zero (as shown in the zoomed section in Figure 17), indicating that DEAIH at the ambient temperature absorbed CO_2 rapidly.

Equations (2), (5), (6), (8) and the equations mentioned in previous studies [4, 5] were used for the calculation of CO_2 in various states. The percent amount of CO_2 varied in gas hydrate, dissolved in water, absorbed in DEAIH, and in gaseous state during the cycle as shown in Figure 18. CO_2 in DEAIH became gaseous CO_2 during regeneration, which was followed by the dissolution of CO_2 in water when CO_2 gas was let to the reactor. The dissolved CO_2 accounted for 9% of the total amount of CO_2 in the system. The CO_2 hydrate formation started at about 145 min and the amount of CO_2 in hydrate gradually grew. The maximum amount of hydrated CO_2 accounted for 14% of the total. At the end, released CO_2 from hydrate dissociation was let back to the CO_2 storage cylinder, where it was absorbed by DEAIH to up to 87% of the total amount of CO_2 in the system. This amount of CO_2 is sufficiently high to allow the following cycle of the coupled system. It is noted that the pressure and temperature in the system should be controlled as to avoid re-absorption of CO_2 in DEAIH during CO_2 regeneration and to meet the CO_2 hydrate formation and dissociation conditions. The gaseous CO_2 is of the largest proportion in the system to provide a pressure high enough to trigger CO_2 hydrate formation. However, it may lead to a waste of materials and space, and therefore the system needs to be optimised in practical designs.

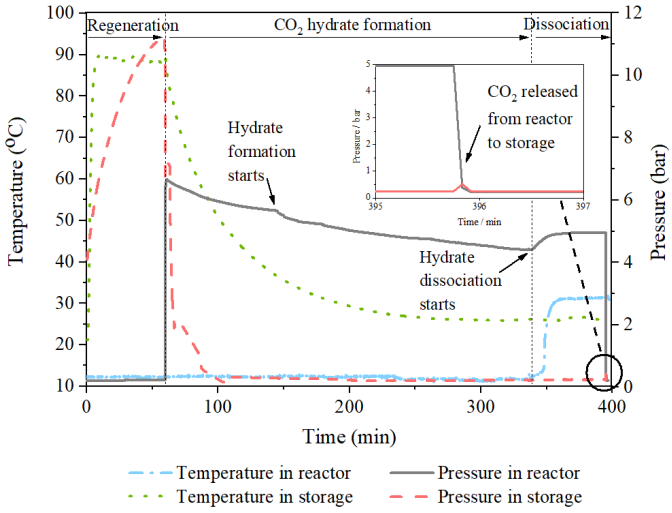

Figure 17. Temperature and pressure in reactor and storage.

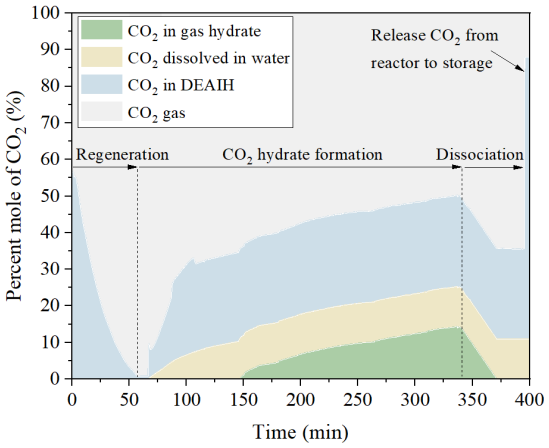

Figure 18. Amount of CO_2 in hydrate, water, DEAIH and gas during the operation.

5 Conclusions

Hydrogels ensure that the CO_2–amine reactions are maintained with significantly increased interfacial area and absorption kinetics. A CO_2 gas storage enabled by amine diethanolamine infused hydrogels (DEAIH) was studied and coupled with a CO_2 hydrate-based cold thermal energy storage. The effects of pressure, temperature, DEAIH sample mass and amine diethanolamine (DEA) concentration on the CO_2 absorption performance of DEAIH were studied. A higher pressure was found to prompt CO_2 absorption while a temperature of 12°C resulted in the highest CO_2 absorption rate. At concentrations above 30 wt%, a lower DEA concentration was favourable to maintain a high normalised CO_2 absorption and absorption rate. In the regeneration at zero gauge pressure, a higher regeneration temperature was favourable for CO_2 regeneration. In the regeneration at non-zero gauge pressures, the pressure rise caused by CO_2 regeneration was followed by a pressure drop due to re-absorption. The system passed through a meta-equilibrium before it reached the equilibrium pressure. The CO_2 regeneration was lowered with increasing the gauge pressure. Cyclic absorption and regeneration at 110°C under zero gauge pressure showed the capacity of DEAIH to absorb CO_2 decreased dramatically after the third run, which was mainly attributed to the volatility of DEA. DEAIH was found to be possible for cyclic CO_2 storage in CO_2 hydrate-based cold thermal energy storage through the operations of the coupled system. Generalised DEAIH-based CO_2 storage can be designed for cooling applications such as refrigeration, dehumidification, and solar absorption and adsorption cooling. Although it is widely admitted that the temperature swing method is energy consuming, this application with low and high-temperature parts can be high-efficiency if implemented systems with low-cost heat source for CO_2 regeneration. An example is solar thermal-adsorption/absorption cooling system with chilled water for CO_2 hydrate-based CTES and stored solar hot water for CO_2 regeneration. The system performance can be a topic of future work. In addition, for cold storage use, the coupled system in

a practical air conditioning system is operated on a daily basis. Theoretically, without CO_2 leakage, the cyclic operations can be well maintained. For small leakage of CO_2 over time, CO_2 must be compensated between each run. Therefore, for future work, the energy efficiency and the amount of CO_2 compensation can be optimised via appropriate control strategies.

Acknowledgement

We thank Mahdiar Taheri, Hongjun Chen and Yimeng Zhang for assisting with the experimental work. Dr Xiaolin Wang is the recipient of an Australian Research Council Discovery Early Career Researcher Award (project number DE200100326) funded by the Australian Government.

Reference

[1] Zhai, X.Q., Wang, X.L., Wang, T., Wang, R.Z., 2013. A review on phase change cold storage in air-conditioning system: Materials and applications. Renewable and Sustainable Energy Reviews 22, 108–120.

[2] Fournaison, L., Delahaye, A., Chatti, I., Petitet, J.P., 2004. CO_2 Hydrates in Refrigeration Processes. Industrial & Engineering Chemistry Research 43(20), 6521–6526.

[3] Kim, S., Lee, S.H., Kang, Y.T., 2017. Characteristics of CO_2 hydrate formation/dissociation in H_2O + THF aqueous solution and estimation of CO_2 emission reduction by district cooling application. Energy 120, 362–373.

[4] Wang, X., Dennis, M., 2016. Phase equilibrium and formation behaviour of CO_2-TBAB semi-clathrate hydrate at low pressures for cold storage air conditioning applications. Chemical Engineering Science 155, 294–305.

[5] Wang, X., Dennis, M., 2017. Phase Equilibrium and Formation Behavior of the CO_2–TBPB Semiclathrate Hydrate for Cold Storage Applications. Journal of Chemical & Engineering Data 62(3), 1083–1093.

[6] Arjmandi M., Chapoy A., Tohidi B., 2007. Equilibrium Data of Hydrogen, Methane, Nitrogen, Carbon Dioxide, and Natural Gas in Semi-Clathrate Hydrates of Tetrabutyl Ammonium Bromide. J. Chem. Eng. Data, 52, 2153–2158.

[7] Mayoufi N., Dalmazzone D., Delahaye A., Clain P., Fournaison L., Furst W., 2011. Experimental Data on Phase Behavior of Simple Tetrabutylphosphonium Bromide (TBPB) and Mixed CO_2+TBPB Semiclathrate Hydrates. J. Chem. Eng. Data, 56, 2987–2993.

[8] Kang S.P., Lee H., Lee C.S., Sung W.M., 2001. Hydrate phase equilibria of the guest mixtures containing CO_2, N_2 and tetrahydrofuran. Fluid Phase Equilibria 185, 101–109.

[9] Wang X. 2016. Carbon dioxide semi-clathrate hydrate for cold storage based air conditioning systems: materials and applications. PhD Thesis. The Australian National University. Canberra.

[10] Wang, X., Zhang, F., Lipiński, W., 2020. Carbon dioxide hydrates for cold thermal energy storage: A review. Solar Energy 211, 11–30.

[11] Gambelli A.M., 2021. An experimental description of the double positive effect of CO_2 injection in methane hydrate deposits in terms of climate change mitigation. Chemical Engineering Science, 233, 116430.

[12] Yuan Q., Sun C.Y., Yang X., Ma P.C., Ma Z.W., Liu B., Ma Q.L., Yang L.Y., Chen G.J., 2021. Recovery of methane from hydrate reservoir with gaseous carbon dioxide using a three-dimensional middle-size reactor. Energy, 40, 47–58.

[13] Wang, X., Dennis, M., 2017. Charging performance of a CO_2 semi-clathrate hydrate based PCM in a lab scale cold storage system. Applied Thermal Engineering 126, 762–773.

[14] Wang, X., Dennis, M., 2017. Thermal energy harvest in the discharge of CO_2 semi-clathrate hydrate in an emulated cold storage system. Applied Thermal Engineering 124, 725–733.

[15] Ma, Z.W., Zhang, P., Bao, H.S., Deng, S., 2016. Review of fundamental properties of CO_2 hydrates and CO_2 capture and separation using hydration method. Renewable and Sustainable Energy Reviews 53, 1273–302.

[16] Dawson, R., Cooper, A.I., Adams, D.J., 2011. Nanoporous organic polymer networks. Progress in Polymer Science 37, 530–563.

[17] Woodward, R.T., Stevens, L.A., Dawson, R., Vijayaraghavan, M., Hasell, T., Silverwood, I.P., et al, 2014. Swellable, Water- and Acid-Tolerant Polymer Sponges for Chemoselective Carbon Dioxide Capture. Journal of the American Chemical Society 136, 9028–35.

[18] Yang, Y., Tan, B., Wood, C.D., 2016. Solution-processable hypercrosslinked polymers by low cost strategies: a promising platform for gas storage and separation. Journal of Materials Chemistry A 4, 15072–80.

[19] Barzagli, F., Lai, S., Mani, F., 2014. Novel non-aqueous amine solvents for reversible CO_2 capture. Energy Procedia 63, 1795–804.

[20] Zhang, F., Zhou, Y., Sun, W., Hou, S., Yu, L., 2018. CO_2 capture from reheating furnace based on the sensible heat of continuous casting slabs. International Journal of Energy Research 42, 2273–83.

[21] Kalatjari, H.R., Haghtalab, A., Jafari Nasr M.R., Heydarinasab, A., 2019. Experimental, simulation and thermodynamic modeling of an acid gas removal pilot plant for CO_2 capturing by mono-ethanol amine solution. Journal of Natural Gas Science and Engineering 72, 103001.

[22] Seo, S., Lages, B., Kim, M., 2020. Catalytic CO_2 absorption in an amine solvent using nickel nanoparticles for post-combustion carbon capture. Journal of CO_2 Utilization 36, 244–252.

[23] Ding, J., Freeman, B., Rochelle, G.T., 2017. Regeneration Design for NGCC CO_2 Capture with Amine-only and Hybrid Amine/Membrane. Energy Procedia 114, 1394–1408.

[24] Sneddon, G., Greenaway, A., You, H.H.P., 2014. The Potential Applications of Nanoporous Materials for the Adsorption, Separation, and Catalytic Conversion of Carbon Dioxide. Advanced Energy Materials 4, 1301873.

[25] Djeridi W., Ben Mansour, N., Ouederni, A., Llewellyn, P.L., El Mir, L., 2017. Study of methane and carbon dioxide adsorption capacity by synthetic nanoporous carbon based on pyrogallol-formaldehyde. International Journal of Hydrogen Energy 42, 8905–13.

[26] Saha, D., Orkoulas, G., Chen, J., Hensley, D.K., 2017. Adsorptive separation of CO_2 in sulfur-doped nanoporous carbons: Selectivity and breakthrough simulation. Microporous and Mesoporous Materials 241, 226–37.

[27] Meng, L.Y., Park, S.J., 2014. Effect of $ZnCl_2$ activation on CO_2 adsorption of N-doped nanoporous carbons from polypyrrole. Journal of Solid State Chemistry 218, 90–4.

[28] Zhang, X., Li, W., Lu, A., 2015. Designed porous carbon materials for efficient CO_2 adsorption and separation. New Carbon Materials 30, 481–501.

[29] Lu A.H., Hao G.P., Zhang X.Q., 2014. Porous Carbons for Carbon Dioxide Capture. In: Lu A.H., Dai S. (eds) Porous Materials for Carbon Dioxide Capture. Green Chemistry and Sustainable Technology. Springer, Berlin, Heidelberg.

[30] Singh, G., Ismail, I.S., Bilen, C., Shanbhag, D., Sathish, C.I., Ramadass, K., Vinu, A., 2019. A facile synthesis of activated porous carbon spheres from d-glucose using a non-corrosive activating agent for efficient carbon dioxide capture. Applied Energy 255, 113831.

[31] Qi, S.C., Liu, Y., Peng, A.Z., Xue, D.M., Liu, X., Liu, X.Q., Sun, L.B., 2019. Fabrication of porous carbons from mesitylene for highly efficient CO_2 capture: A rational choice improving the carbon loop. Chemical Engineering Journal 361, 945–952.

[32] Wei, H., Chen, H., Fu, N., Chen, J., Lan, G., Qian, W., Liu, Y., Lin, H., Han, S., 2017. Excellent electrochemical properties and large CO_2 capture of nitrogen-doped activated porous carbon synthesised from waste longan shells. Electrochimica Acta 231, 403–411.

[33] He, Y., Shang, J., Zhao, Q., Gu, Q., Xie, K., Li, G., Singh, R., Xiao, P., Webley, P.A., 2016. A comparative study on conversion of porous and non-porous metal–organic frameworks (MOFs) into carbon-based composites for carbon dioxide capture. Polyhedron 120, 30–35.

[34] Shi, P., Chen, X., Sun, Z., Li, C., Xu, Z., Jiang, X., Jiang, B., 2020. Thickness controllable hypercrosslinked porous polymer nanofilm with high CO_2 capture capacity. Journal of Colloid and Interface Science, 563, 272–280.

[35] Mukhtar, A., Saqib, S., Mellon, N.B, Babar, M., Rafiq, S., Ullah, S., Bustam, M.A., Al-Sehemi, A.G., Muhammad, N., Chawla, M., 2020. CO_2 capturing, thermo-kinetic principles, synthesis and amine functionalization of covalent organic polymers for CO_2 separation from natural gas: A review. Journal of Natural Gas Science and Engineering 77, 103203.

[36] Varghese, A.M., Karanikolos, G.N., 2020. CO_2 capture adsorbents functionalized by amine – bearing polymers: A review. International Journal of Greenhouse Gas Control 96, 103005.

[37] Yang, X., Rees, R.J., Conway, W., Puxty, G., Yang, Q., Winkler, D.A., 2017. Computational Modeling and Simulation of CO_2 Capture by Aqueous Amines. Chem. Rev 117, 14, 9524–9593.

[38] Xu, C., Yang, Y., Acencios Falcon, L.P., Hazewinkel, P., Wood, C.D., 2019. Carbon capture by DEA-infused hydrogels. International Journal of Greenhouse Gas Control 88, 226–232.

[39] Chen, C., Kim, J., Ahn, W.S., 2014. CO_2 capture by amine-functionalized nanoporous materials: A review. Korean Journal of Chemical Engineering 31, 1919–34.

[40] Chen, C., Bhattacharjee, S., 2017. Trimodal nanoporous silica as a support for amine-based CO_2 adsorbents: Improvement in adsorption capacity and kinetics. Applied Surface Science 396, 1515–9.

[41] Anbia, M., Hoseini, V., 2012. Enhancement of CO_2 adsorption on nanoporous chromium terephthalate (MIL-101) by amine modification. Journal of Natural Gas Chemistry 21, 339–43.

[42] Gao, J., Hoshino, Y., Inoue, G., 2020. Honeycomb-carbon-fiber-supported amine-containing nanogel particles for CO_2 capture using a rotating column TVSA. Chemical Engineering Journal 383, 123123.

[43] Xu, X., Heath, C., Pejcic, B., Wood, C.D., 2018. CO_2 capture by amine infused hydrogels (AIHs), Journal of Materials Chemistry A 6(11), 4829–4838.

[44] Mahon, R., Balogun, Y., Oluyemi, G. Njuguna, J., 2020. Swelling performance of sodium polyacrylate and poly(acrylamide-co-acrylic acid) potassium salt. SN Applied Sciences 2, 117.

[45] Wang, X., Dennis, M., Jiang, J., Zhou, L., Zhai, X., Lipinski, W., 2019. Performance of a novel cold thermal storage material in an emulated air conditioning system using different storage strategies. International Journal of Refrigeration 104, 259–269.

[46] Anderson, Graydon K., 2002. Solubility of carbon dioxide in water under incipient clathrate formation conditions. J.ChemEng.Data 47(2), 219–222.

[47] Diamond, Larryn W., Akinfiev, Nikolay N., 2003. Solubility of CO_2 in water from –1.5 to 100°C and from 0.1 to 100 MPa: evaluation of literature data and thermodynamic modelling. Fluid Phase Equilib. 208(1–2), 265–290.

[48] Carroll, John J., Slupsky, John D., Mather, Alan E., 1991. The solubility of carbon dioxide in water at low pressure. J. Phys. Chem Ref. Data 20, 1201–1208.

[49] Marinhas, S., Delahaye, A., Fournaison, L., et al., 2006. Modelling of the available latent heat of a CO_2 hydrate slurry in an experimental loop applied to secondary refrigeration. Chemical Engineering and Processing: Process Intensification 45(3), 184–192.

[50] Yu, J., Zhai, Y., Chuang, S.S.C., 2018. Water enhancement in CO_2 capture by amines: an insight into CO_2−H_2O interactions on amine films and sorbents. Industrial & Engineering Chemistry Research 57, 4052–4062.

[51] Jos Oomens, Jeffrey D. Steill. Free Carboxylate Stretching Modes, 2008. The Journal of Physical Chemistry A 112(15):3281–3.

[52] Udara S.P.R. Arachchige, Neelakantha Aryal, Dag A. Eimer, Morten C. Melaaen., 2013. Viscosities of Pure and Aqueous Solutions of Monoethanolamine (MEA), Diethanolamine (DEA) and N-Methyldiethanolamine (MDEA). Annual Transactions of the Nordic Rheology Society, 21.

[53] Xue, B., Yu, Y., Chen, J. et al, 2017. A comparative study of MEA and DEA for post-combustion CO_2 capture with different process configurations. International Journal of Coal Science & Technology 4, 15–24.

[54] Vega, F., Cano, M., Camino, S., Gallego Fernández, L.M., Portillo, E., Navarrete, B. (August 16th 2018). Solvents for Carbon Dioxide Capture, Carbon Dioxide Chemistry, Capture and Oil Recovery, Iyad Karamé, Janah Shaya and Hassan Srour, IntechOpen, DOI: 10.5772/intechopen.71443.

[55] Zhang W., Liu H., Sun Y., Cakstins J., Sun C., Snape C.E., 2016. Parametric study on the regeneration heat requirement of an amine-based solid adsorbent process for post-combustion carbon capture. Applied Energy 168(15), 394–405.

[56] Hauchhum, L., Mahanta, P. Carbon dioxide adsorption on zeolites and activated carbon by pressure swing adsorption in a fixed bed. Int J Energy Environ Eng 5, 349–356 (2014).

[57] Augustine Ntiamoah, Jianghua Ling, Penny Xiao, Paul A. Webley, Yuchun Zhai. CO_2 Capture by Temperature Swing Adsorption: Use of Hot CO_2-Rich Gas for Regeneration. Ind. Eng. Chem. Res. 2016, 55, 703−713.

[58] Jarad A. Mason, Kenji Sumida, Zoey R. Herm, Rajamani Krishna, Jeffrey. R. Long. Evaluating metal–organic frameworks for post-combustion carbon dioxide capture via temperature swing adsorption. Energy Environ. Sci., 2011, 4, 3030.

[59] Carbon Engineering. 2021. Carbon Engineering | Direct Air Capture of CO2 | Home. [online] Available at: <https://carbonengineering.com/> [Accessed 2 July 2021].

[60] L Reich, L Yue, R Bader, W Lipiński. Towards solar thermochemical carbon dioxide capture via calcium oxide looping: A review. Aerosol and Air Quality Research 14 (2), 500-514.